


## Article

# Coating Characteristic of Hydroxyapatite on Titanium Substrates via Hydrothermal Treatment

Pham Trung Kien <sup>1,2,3,\*</sup> , Tran Ngo Quan <sup>1,2</sup> and Le Huynh Tuyet Anh <sup>1,2</sup>

<sup>1</sup> Faculty of Materials Technology, Ho Chi Minh City University of Technology (HCMUT), 268 Ly Thuong Kiet Street, District 10, Ho Chi Minh City 008428, Vietnam; tnquan.sdh20@hcmut.edu.vn (T.N.Q.); tuyetanhllh@hcmut.edu.vn (L.H.T.A.)

<sup>2</sup> Vietnam National University Ho Chi Minh City (VNUHCM), Linh Trung Ward, Thu Duc District, Ho Chi Minh City 008428, Vietnam

<sup>3</sup> Polymer Research Center, Ho Chi Minh City University of Technology (HCMUT), 268 Ly Thuong Kiet Street, District 10, Ho Chi Minh City 008428, Vietnam

\* Correspondence: phamtrungkien@hcmut.edu.vn; Tel.: +84-908-661-076

**Abstract:** Medical pure titanium (Ti) shows excellent chemical stability and mechanical properties in clinical uses, but its initial fixation with host bone, when implanted, is usually delayed owing to the bioinert Ti surface. In this study, we fabricate the hydroxyapatite (HA)-coated titanium by three steps reactions: (1) to form an activated  $O^{2-}$  layer by immersing Ti substrate into an alkaline solution such as NaOH; (2) the  $O^{2-}$  bonds with  $Ca^{2+}$  to form Ca–O–Ti bonding, in which O plays the part of bridge materials between Ca and Ti substrate and (3) the conversion of Ca–O–Ti samples to HA-coated Ti samples by immersion into  $Na_2HPO_4$  2 M at 180 °C for 48 h using hydrothermal methods. The effect of different phosphate solutions ( $NaH_2PO_4$  2 M and  $Na_2HPO_4$  2 M solution) and hydrothermal treatment time (24 and 48 h) on the characteristic of hydroxyapatite coating titanium substrate is also investigated using the optical microscope, thin film XRD and SEM/EDX. The HA-coated Ti samples fabricated by immersion into  $Na_2HPO_4$  2 M at 180 °C for 48 h show fiber HA covering Titan substrate with a diameter varying from 0.1 to 0.3  $\mu m$ . These HA-coated Ti samples can be regarded as promising multifunctional biomaterials.

**Keywords:** hydroxyapatite coating; titanium; hydrothermal treatment; bone implant



**Citation:** Kien, P.T.; Quan, T.N.; Tuyet Anh, L.H. Coating Characteristic of Hydroxyapatite on Titanium Substrates via Hydrothermal Treatment. *Coatings* **2021**, *11*, 1226. <https://doi.org/10.3390/coatings11101226>

Academic Editor: Simona Liliana Iconaru

Received: 16 August 2021  
Accepted: 30 September 2021  
Published: 9 October 2021

**Publisher's Note:** MDPI stays neutral with regard to jurisdictional claims in published maps and institutional affiliations.



**Copyright:** © 2021 by the authors. Licensee MDPI, Basel, Switzerland. This article is an open access article distributed under the terms and conditions of the Creative Commons Attribution (CC BY) license (<https://creativecommons.org/licenses/by/4.0/>).

## 1. Introduction

Historically, titanium (Ti) has been used widely to develop artificial bone graft implants for a long time due to its high bioinert properties, long-term implant corrosion resistance, high mechanical strength and biocompatibility [1–3]. Despite the fact that titanium has been used widely in clinical settings, e.g., dental and orthopedic implants, a favorable bioactivity performance was not always obtained upon contact with the bone [4,5]. Forming an inert  $TiO_2$  layer on the surface of a Ti substrate upon exposure to oxygen decreases the bioactivity of the Ti implant and delays the fixation of the osteoblast cells to the Ti surface [6–12]. Since titanium was reported to be an excellent biocompatible material in animal studies, the commercially pure titanium is the most prominent alloy used for biomedical applications.

These Ti materials are widely used due to their high Young's modulus when compared to human bone, eminent biocompatibility, machinability, formability, compatibility, corrosion, and crack resistance, as well as their remarkable bending and fatigue strength [13,14]. These properties make titanium and its alloy ideal for bone and joint or cochlear replacements, orthodontic surgery screw parts, tooth fixation dental implants, artificial heart valves, and surgical instruments [15,16].

In addition, the higher mechanical strength of Ti samples could release the residual stress on implanted bone during body movement after bone treatment [17]. To avoid these

disadvantages of pure titanium implants as well as accelerate the fixation of the Ti implant to the host bone, the Ti implant surface needs to be bonded with a calcium and phosphate (CaP) layer based on the concept that the CaP layer with a chemical composition similar to host bone could obtain better bond between the CaP coated titanium and host bone. Among these CaP materials, hydroxyapatite ( $\text{Ca}_{10}(\text{PO}_4)_6(\text{OH})_2$ ) (HA) has been selected as a good choice owing to its excellent bioactivity [18–24]. Therefore, the need to fabricate an HA-coated titanium substrate for bone regeneration has received significant attention recently. To prepare the HA and calcium phosphate materials, researchers refer to the chemical route such as the precipitation method, the hydrothermal method, due to its simplicity, and the cost-effective method to apply in mass production [25–30]. Thus, we aim to coat HA on the pure titanium substrate by immobilizing the  $\text{Ca}^{2+}$  ion onto the titanium surface, then immersing it into phosphate solution to form a CaP coating layer on the Ti surface using hydrothermal treatment. In this study, we fabricated the HA-coated Titan substrate by hydrothermal reaction. We also investigate the effect of different phosphate ( $\text{H}_3\text{PO}_4$  15 M,  $\text{NaH}_2\text{PO}_4$  2 M and  $\text{Na}_2\text{HPO}_4$  2 M) solutions and hydrothermal treatment times (180 °C for 24 and 48 h) characteristic of a hydroxyapatite-coated titanium substrate.

## 2. Materials and Methods

### 2.1. Materials

The commercial Ti substrates (smooth Ti) measuring 12 mm (length)  $\times$  5 mm (width)  $\times$  5 mm (height) were donated from the Department of Orthopedics, Cho Ray Hospital, Ho Chi Minh City, Vietnam. Sulfuric acid, hydrochloric acid,  $\text{Ca}(\text{NO}_3)_2 \cdot 4\text{H}_2\text{O}$ ,  $\text{H}_3\text{PO}_4$ ,  $\text{NaH}_2\text{PO}_4$  and  $\text{Na}_2\text{HPO}_4$  materials were supplied by Xilong Chemical (Chengdu, China) without purification.

### 2.2. Preparation of Rough-Surface Ti Samples

Smooth surface Ti was chemically etched using the mixture of 50% vol sulfuric acid and 7% vol hydrochloric acid at 70 °C for 30 min with the volume ratio of  $\text{H}_2\text{SO}_4$ :HCl as 50:50. Then, the obtained rough Ti was washed ultrasonically with ethanol and distilled water each for 5 min successively, followed by drying overnight.

### 2.3. Preparation of Ca–O–Ti Samples

The rough-surface Ti bars were immersed in NaOH 5 M at 60 °C for 24 h, followed by immersion in  $\text{Ca}(\text{NO}_3)_2 \cdot 4\text{H}_2\text{O}$  0.5 M at 60 °C for 1 h to achieve the Ca–O–Ti uniform coating. The evaporation of solvent resulted in the precipitation of  $\text{Ca}(\text{NO}_3)_2$  on the surface of rough Ti bars. The rough Ti coated with  $\text{Ca}(\text{NO}_3)_2$  was heated at 600 °C for 3 h with the heating ratio of 10 °C/min using an electric furnace (Nabertherm 1400, Berlin, Germany) to obtain the Ca–O–Ti bars. During the heat treatment,  $\text{Ca}(\text{NO}_3)_2$  was thermally decomposed to CaO, and the CaO subsequently reacted with the  $\text{OH}^-$  group on the rough-surface Ti bars to form Ca–O–Ti samples. The Ca–O–Ti samples were cooled down in the furnace before removal to release the residual stress of coating within.

### 2.4. Preparation of Hydroxyapatite-Coated Ti Samples (HA-Coated Ti Samples)

The Ca–O–Ti bars were immersed in 3 kinds of phosphate solutions at different hydrothermal conditions such as:  $\text{H}_3\text{PO}_4$  15M at 180 °C for 24 h;  $\text{NaH}_2\text{PO}_4$  2 M at 180 °C for 24 and 48 h; and  $\text{Na}_2\text{HPO}_4$  2 M at 180 °C for 24 and 48 h to study the effect of different phosphate solutions on the characteristics of HA-coated Ti bars. The flowchart of preparation HA-coated Ti bars is summarized in Figure 1.

### 2.5. Materials Characterizations

The phase analysis using thin-film XRD: the sample was put in an XRD machine (Bruker D8 Advance, Bruker, Berlin, Germany) with the 2 $\theta$  scanning from 5 to 60°, operation at 40 kV and 40 mA.

The visible images of samples were obtained by an optical microscope (Olympia CX23) (Olympia, Tokyo, Japan) to evaluate the coating layer on Ti bars.

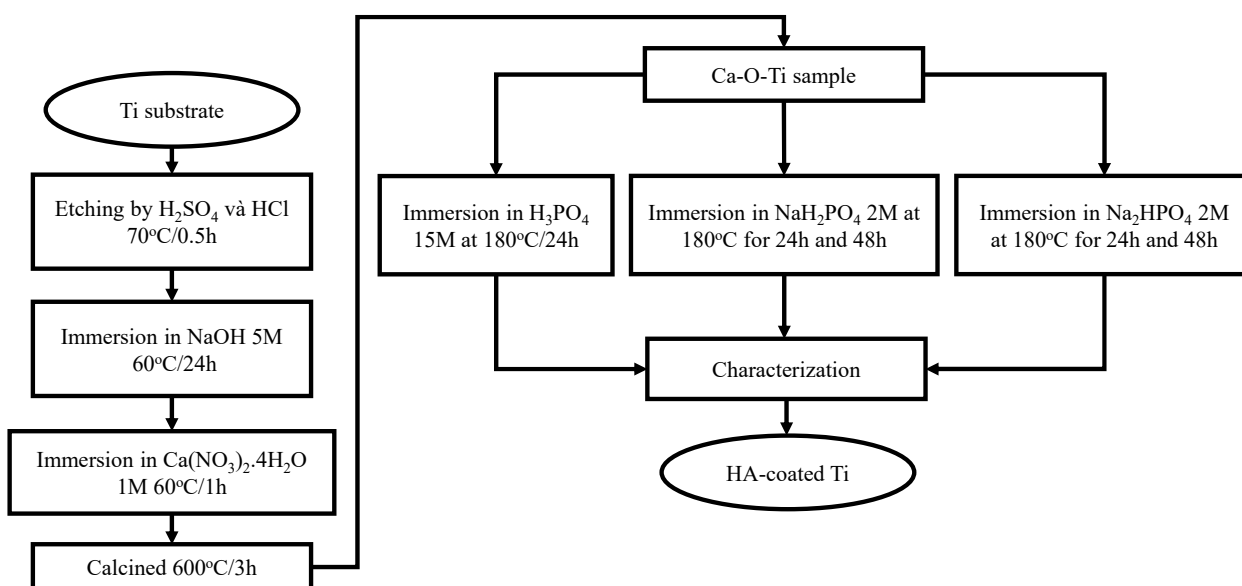


**Figure 1.** Flowchart of preparation HA-coated Ti.

The morphology analysis was performed using SEM/EDX: the sample was adhered with carbon tape stick to copper substrate before carrying out the SEM analysis (Hitachi S-4800) (Hitachi Ltd., Tokyo, Japan) at 10 kV. The elemental mappings of the surface area were observed using the EDX technique, with a focus on Na, P, Ca and Ti elements.

### 3. Results

Figure 2a shows the surface image of the Ti substrate using a microscope technique. In brief, the Ti bar sample has a scratch-free, uniform surface. Table 1 shows the phenomena of Ca–O–Ti bars upon immersion into three kinds of phosphate solutions at 180 °C for different hydrothermal treatment times. When immersed, the Ca–O–Ti samples in phosphoric acid solution 15 M at 180 °C for 24 h, the Ca–O–Ti samples were dissolved completely. In contrast, the shapes of the Ca–O–Ti samples were maintained when immersed in both  $\text{NaH}_2\text{PO}_4$  2 M and  $\text{Na}_2\text{HPO}_4$  2 M solutions at 180 °C for 24 and 48 h as indicated in Table 1. In contrast with uniform Ti substrate (Figure 2a), the Ca–O–Ti samples show different image morphology when immersed in  $\text{NaH}_2\text{PO}_4$  2 M solution at 180 °C for 24 and 48 h. The Ti surface was covered with a white cluster, indicating the new deposition of calcium phosphate crystal on the surface. In addition, these new deposition layers increased when the Ca–O–Ti samples were immersed into  $\text{Na}_2\text{HPO}_4$  2 M solutions at 180 °C for 24 and 48 h (Figure 2c1,c2).

Figure 3 shows the thin film XRD of the Ti substrate (Figure 3a) and Ca–O–Ti samples (Figure 3b) and Ca–O–Ti samples when immersed in different sodium phosphate solutions at 180 °C for 24 and 48 h (Figure 3c1,d1,c2,d2). In brief, the Ti substrate was pure Ti (PDF#44-1294), as shown in Figure 3a, with the strongest peak of Ti at  $2\theta = 40^\circ$ . When immersed into NaOH 5 M at 60 °C for 24 h and  $\text{Ca}(\text{NO}_3)_2 \cdot 4\text{H}_2\text{O}$  1 M at 60 °C for 1 h, followed by calcination at 600 °C for 3 h, the Ti peak could be observed at  $2\theta = 35^\circ$ ,  $38.4^\circ$  and  $40^\circ$ , while the peak of sodium hydrogen titanium oxide ( $\text{Na}_{0.8}\text{H}_{1.2}\text{Ti}_3\text{O}_7$ ) (PDF#48-0693) and perovskite ( $\text{CaTiO}_3$ ) (PDF#22-0153) could be observed at  $2\theta = 29.7^\circ$  and  $32.4^\circ$ , respectively, as shown in Figure 3b. When the Ca–O–Ti samples were treated with  $\text{NaH}_2\text{PO}_4$  2M and  $\text{Na}_2\text{HPO}_4$  solution at 180 °C for 24 h, the peak of sodium hydrogen titanium oxide and perovskite disappeared (Figure 3c1,c2), while the peak of calcium hydrogen phosphite ( $\text{Ca}(\text{H}_2\text{PO}_2)_2$ ) (PDF#01-0588) could be observed at  $2\theta = 26.3^\circ$  (Figure 3c2). In addition, the new peak of hydroxyapatite ( $\text{Ca}_{10}(\text{PO}_4)_6(\text{OH})_2$ ) (PDF#09-0432) could be observed only when Ca–O–Ti samples were immersed in  $\text{Na}_2\text{HPO}_4$  2 M at

180 °C for 48 h, with the 2theta peak of hydroxyapatite at 31.8° (Figure 3d2) as compared with commercial hydroxyapatite (Figure 3e).

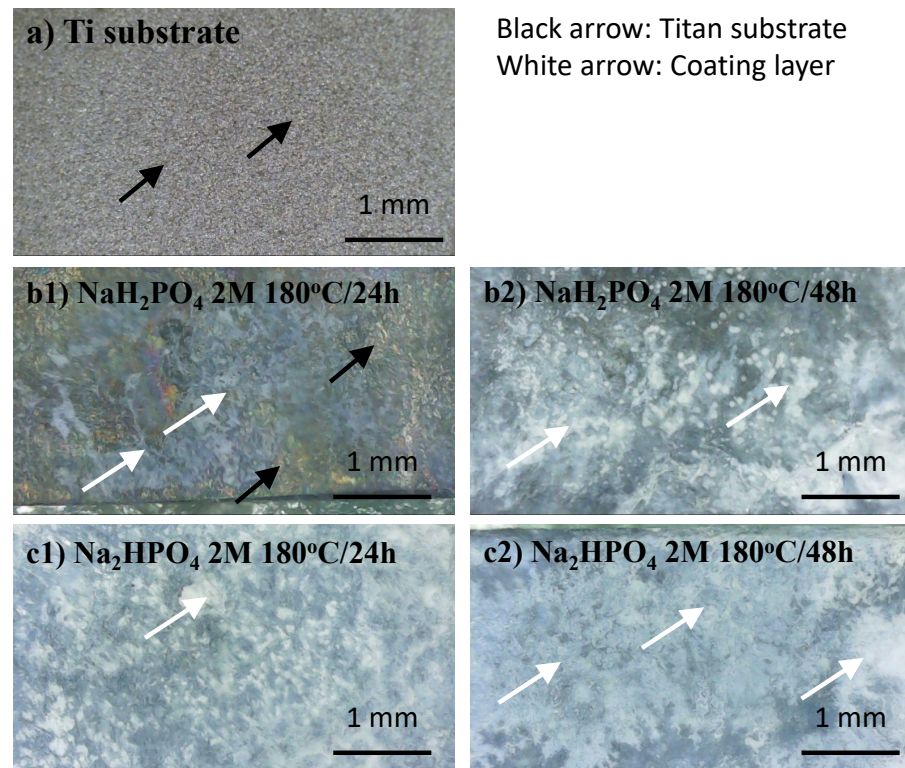


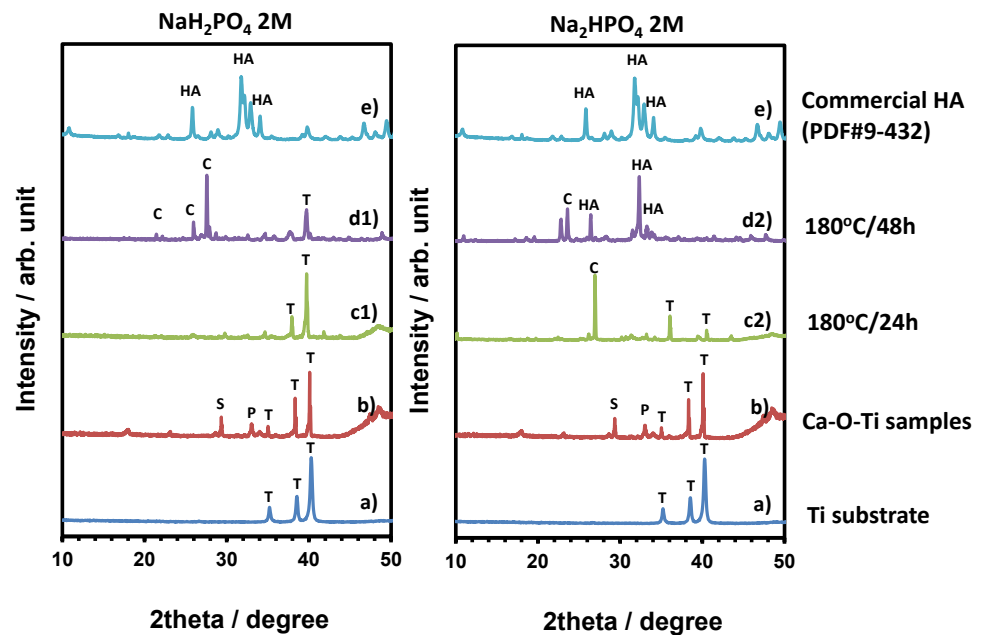
**Figure 2.** Optical microscopy images of (a) Ti bar and when hydrothermally treated at different phosphate solutions: (b1)  $\text{NaH}_2\text{PO}_4$  2 M at 180 °C for 24 h; (b2)  $\text{NaH}_2\text{PO}_4$  2 M at 180 °C for 48 h and (c1)  $\text{Na}_2\text{HPO}_4$  2 M at 180 °C for 24 h; (c2)  $\text{Na}_2\text{HPO}_4$  2 M at 180 °C for 48 h. The black arrows indicate Ti substrate, while the white arrows indicate the coating layer.

**Table 1.** Phenomena observed when Ca–O–Ti bars were immersed into 3 kinds of phosphate solutions at 180 °C for different hydrothermal treatment times.

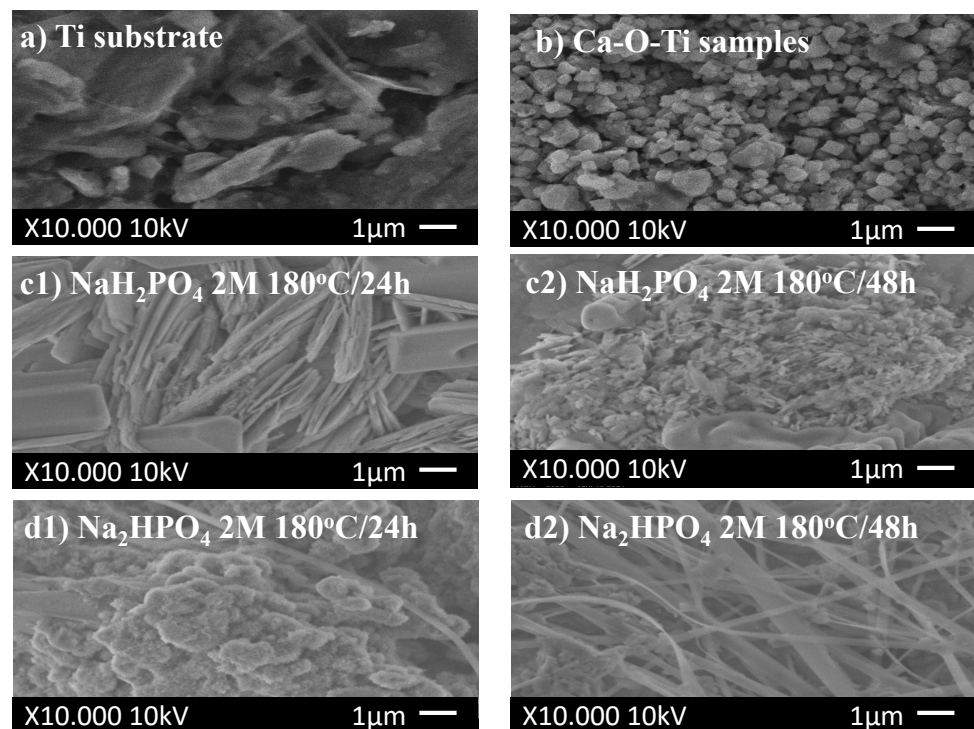
Phosphate Solution	Hydrothermal Treatment Condition	Phenomena Observed by Optical Microscope
$\text{H}_3\text{PO}_4$ 15 M	180 °C for 24 h	Titanium substrate was dissolved
$\text{NaH}_2\text{PO}_4$ 2 M	180 °C for 24 h	The thinner white layer could be observed
	180 °C for 48 h	The thinner white layer could be observed
$\text{Na}_2\text{HPO}_4$ 2 M	180 °C for 24 h	The thicker white layer could be observed
	180 °C for 48 h	The thicker white layer could be observed

Figure 4 shows the SEM images of the Ti substrate (Figure 4a), the Ca–O–Ti samples (Figure 4b) and an SEM image of the Ca–O–Ti sample when immersed in different sodium phosphate solutions at 180 °C for 24 and 48 h (Figure 4c1,d1,c2,d2). In brief, the Ti substrate changed the morphology from plate-like particles (Figure 4a) to irregular particles (Figure 4b) when immersed with  $\text{NaOH}$  5 M and  $\text{Ca}(\text{NO}_3)_2 \cdot 4\text{H}_2\text{O}$  1 M followed by calcination at 600 °C for 3 h. However, when the Ca–O–Ti samples were treated with  $\text{NaH}_2\text{PO}_4$  2 M solution at 180 °C for 24 and 48 h, the morphology changed again from irregular shapes into plate-like shapes (Figure 4c1,c2). In contrast, the Ca–O–Ti samples were treated with  $\text{Na}_2\text{HPO}_4$  2 M solution at 180 °C for 24 and 48 h, the morphology changed from irregular shapes into short and typical long needle-like shapes of hydroxyapatite (Figure 4d1,d2).



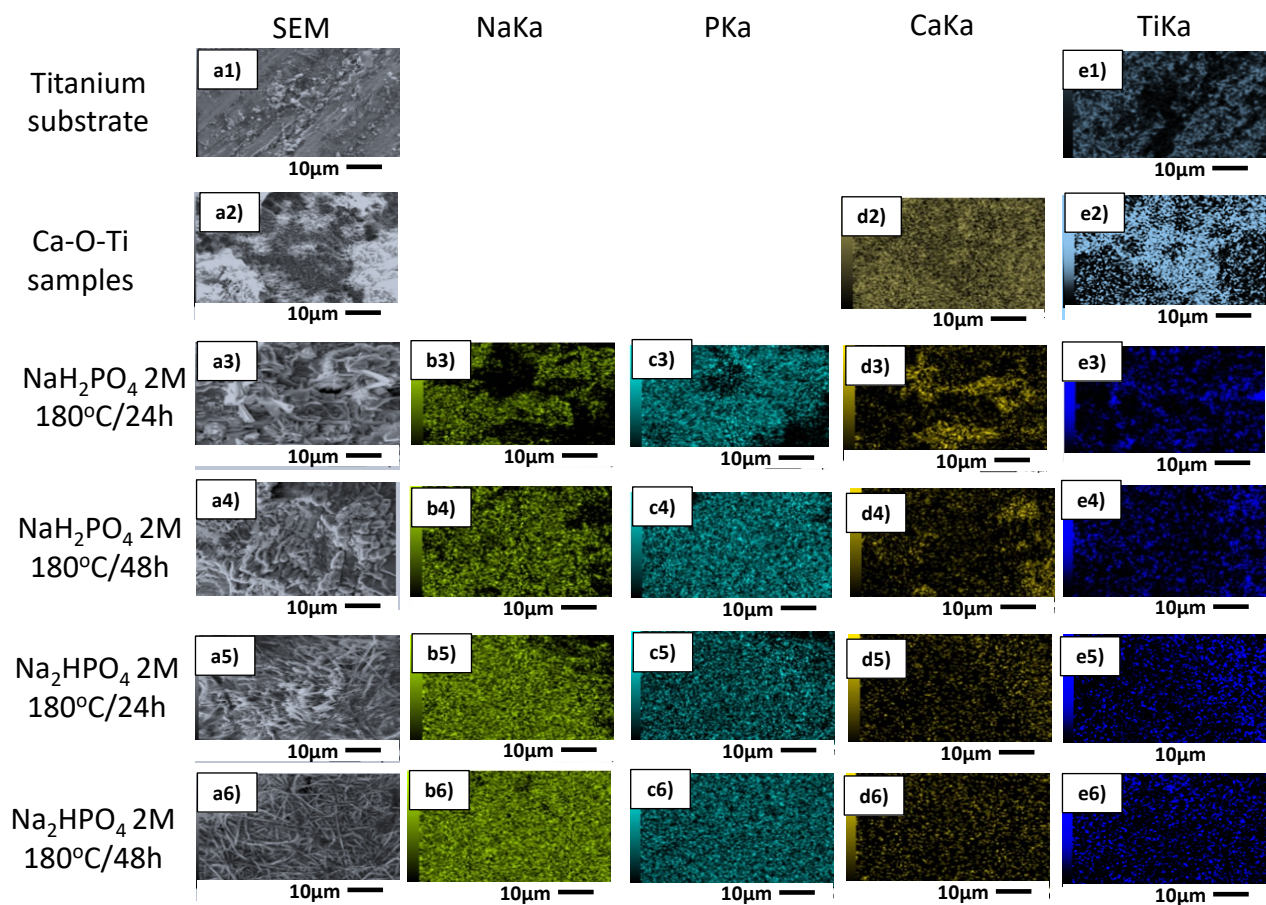


**Figure 3.** Thin film XRD patterns of (a) Ti bar; (b) Ca–O–Ti bar; and when hydrothermally treated with different phosphate solutions, such as (c1)  $\text{NaH}_2\text{PO}_4$  2 M at 180 °C for 24 h; (c2)  $\text{Na}_2\text{HPO}_4$  2 M at 180 °C for 24 h; (d1)  $\text{NaH}_2\text{PO}_4$  2 M at 180 °C for 48 h; (d2)  $\text{Na}_2\text{HPO}_4$  2 M at 180 °C for 48 h and (e) the commercial hydroxyapatite powder. Code: T—titanium (Ti) (PDF#44-1294); S—sodium hydrogen titanium oxide ( $\text{Na}_{0.8}\text{H}_{1.2}\text{Ti}_3\text{O}_7$ ) (PDF#48-0693); P—perovskite ( $\text{CaTiO}_3$ ) (PDF#22-0153); C—calcium hydrogen phosphite ( $\text{Ca}(\text{H}_2\text{PO}_2)_2$ ) (PDF#01-0588); HA—hydroxyapatite ( $\text{Ca}_{10}(\text{PO}_4)_6(\text{OH})_2$ ) (PDF#09-0432).



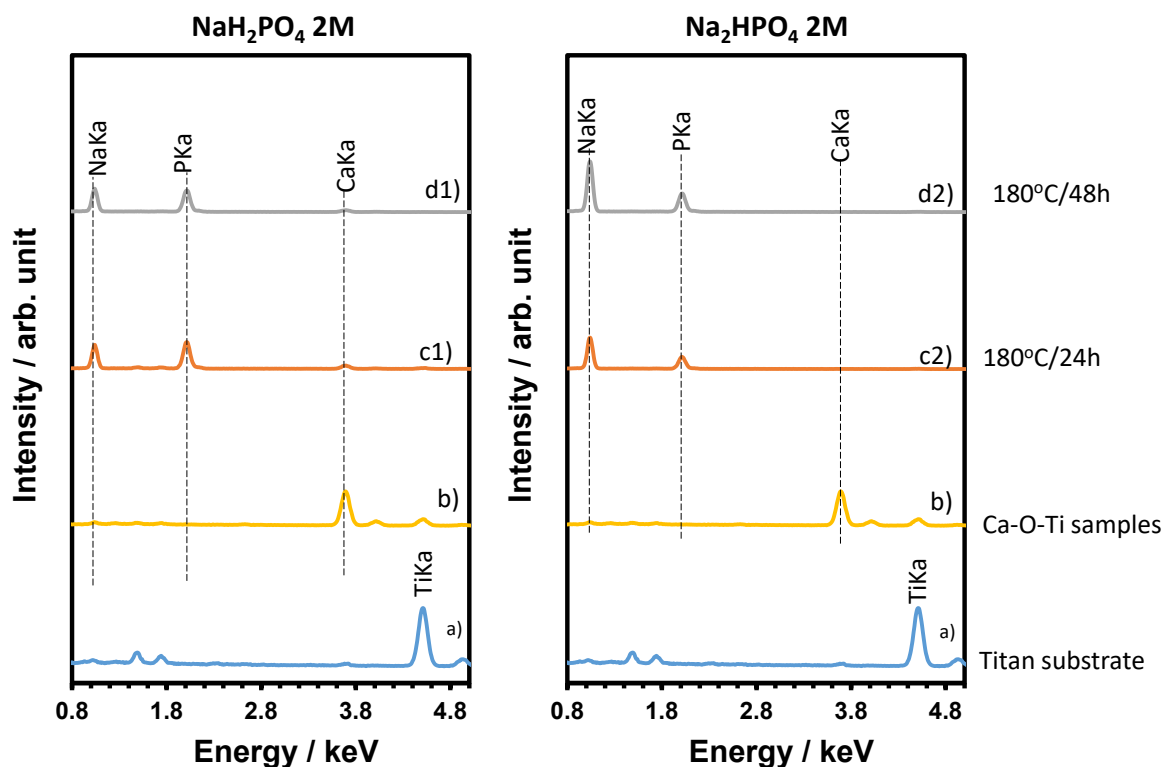
**Figure 4.** SEM images of (a) Ti bar; (b) Ca–O–Ti bar; and when hydrothermal treated at different phosphate solutions such as (c1,c2)  $\text{NaH}_2\text{PO}_4$  2 M at 180 °C for 24 and 48 h; (d1,d2)  $\text{Na}_2\text{HPO}_4$  2 M at 180 °C for 24 and 48 h.

Figure 5 shows the EDX images with mapping elements of NaKa; PKa; CaKa and TiKa of Ti substrate (Figure 5a1,e1), the Ca–O–Ti samples (Figure 5a2,d2,e2) and Ca–O–Ti sample when immersed in different sodium phosphate solutions at 180 °C for 24 and 48 h (Figure 5a3–e3;a4–e4;a5–e5;a6–e6). Basically, the mapping peak of NaKa and PKa increased as Ca–O–Ti samples were immersed in sodium phosphate solutions at 180 °C for 24 and 48 h. In addition, the mapping peak of CaKa reduced as the Ca–O–Ti samples were immersed in sodium phosphate solutions at 180 °C for 24 and 48 h. It needs to be noticed that the distribution of the CaKa peaks was less homogenous when Ca–O–Ti samples were immersed in  $\text{NaH}_2\text{PO}_4$  2 M solution (Figure 5d3,d4) than in  $\text{Na}_2\text{HPO}_4$  solution (Figure 5d5,d6).



**Figure 5.** SEM and EDX images of (a1–e1) Ti substrate; (a2–e2) Ca–O–Ti samples, and when hydrothermally treated with different phosphate solutions; (a3–e3)  $\text{NaH}_2\text{PO}_4$  180 °C/24 h; (a4–e4)  $\text{NaH}_2\text{PO}_4$  180 °C /48 h; (a5–e5)  $\text{Na}_2\text{HPO}_4$  180 °C /24 h and (a6–e6)  $\text{Na}_2\text{HPO}_4$  180 °C /48h.

Figure 6 shows the EDX spectra of the NaKa, PKa, CaKa and TiKa elements of the Ti substrate (Figure 6a), the Ca–O–Ti samples (Figure 6b) and the Ca–O–Ti sample when immersed in different sodium phosphate solutions at 180 °C for 24 (Figure 6(c1,c2)) and 48 h (Figure 6(d1,d2)). Basically, the titanium substrates demonstrated a TiKa peak at energy = 4.7 keV (Figure 6a). The Ca–O–Ti sample exposed the CaKa peak at energy = 3.8 keV and a small TiKa peak at energy = 4.7 keV (Figure 6b), indicating that the titanium substrates were completely covered by a calcium layer. In addition, the Ca–O–Ti samples treated by  $\text{NaH}_2\text{PO}_4$  2 M and  $\text{Na}_2\text{HPO}_4$  2 M at 180 °C for 24 and 48 h displayed the NaKa, PKa and CaKa peak at energy = 1, 2.1 and 3.8 keV, respectively (Figure 6(c1,d1,c2,d2)). However, in the case of using  $\text{Na}_2\text{HPO}_4$  2 M solution, the peak of CaKa was too small to detect, indicating that Ca was immobilized under the PKa layer (Figure 6(c2,d2)).



**Figure 6.** EDX spectra of NaKa, PKa, CaKa and TiKa elements of (a) Ti substrate; (b) the Ca–O–Ti samples; (c1,d1) Ca–O–Ti sample when immersed in the  $\text{NaH}_2\text{PO}_4$  solution at 180 °C for 24 and 48 h and (c2,d2) the Ca–O–Ti sample when immersed in the  $\text{Na}_2\text{HPO}_4$  solution at 180 °C for 24 and 48 h.

#### 4. Discussion

A hydroxyapatite-coated titanium substrate was successfully obtained via the following steps: (1) form an activated  $\text{O}^{2-}$  layer by immersing Ti substrate in alkaline solution, such as NaOH; (2) the  $\text{O}^{2-}$  bonds with  $\text{Ca}^{2+}$  to form a Ca–O–Ti bond, in which O acts as a bridge material between the Ca and Ti substrate. The calcination process supports the immobilization of  $\text{Ca}^{2+}$  in the deep surface of the Ti substrate, enhancing the interlocking between the Ti substrate and  $\text{Ca}^{2+}$ ; (3) convert Ca–O–Ti samples into CaP–Ti samples by immersion in phosphate solution. As a result, the hydroxyapatite deposited on the Ti surface leads to favorable bonding between the Ti surface and bone area contact. The summary mechanisms of the hydroxyapatite coating on the surface of the Ti substrate are introduced in Figure 7.

The soaking process of Titanium substrate into  $\text{Na}_2\text{HPO}_4$  2 M solution at 180 °C for 48 h often involves the supersaturated  $\text{PO}_4^{3-}$  group, leading to the precipitation of hydroxyapatite on the Ti substrate. With regards to the biological activity of the HA-coated Ti sample and pure Ti-sample, the appearance of Ca and P ions immobilized on the Ti surface promotes the fixation of the osteoblast cell on the Ti surface upon initial implantation; thus, the HA-coated Ti sample could be used as bone graft materials. Doe et al. reported that HA-coated Ti implanted in rat long bone promotes the bone formation with superior biocompatibility, stability and biosafety [31]. These findings are also similar with to previous research, which found that the Ti alloy, after coating with nano silver particle (AgNP) and  $\beta$ -TCP, can enhance the viability of MSCs as  $\text{Ca}^{2+}$  and  $\text{PO}_4^{3-}$  are generated after the hydrolysis of  $\beta$ -TCP [32,33]. Ayukawa et al. reported that the osseointegration for titanium is achieved by binding calcium-binding proteins such as osteopontin and osteocalcin to the titanium surface via calcium ion [34]. The meaning of this research should be put into the context of research oriented in the author’s lab. In the present study, the forming of HA on the Ti surface was favorable if Ca–O–Ti samples were immersed in  $\text{Na}_2\text{HPO}_4$  solution at 180 °C for 48 h. Some studies have considered the effect of different

sodium phosphate solutions on the synthesis of HA, for example, Kunio Ishikawa suggests the use of  $\text{Na}_{1.8}\text{H}_{1.2}\text{PO}_4$  can accelerate the forming of HA putty [35]. In the research by Arief, HA was formed by mixing of  $\text{CaCO}_3$  and dicalcium phosphate anhydrous (DCPA:  $\text{CaHPO}_4$ ) and immersing in  $\text{Na}_2\text{HPO}_4$  0.8 M solution (pH 8.2) at 37 °C for 72 h [36]. In this study, the transformation of Ca–O–Ti samples to HA–Ti sample occurred when Ca–O–Ti samples were immersed in  $\text{Na}_2\text{HPO}_4$  2 M solutions at 180 °C for 48 h.

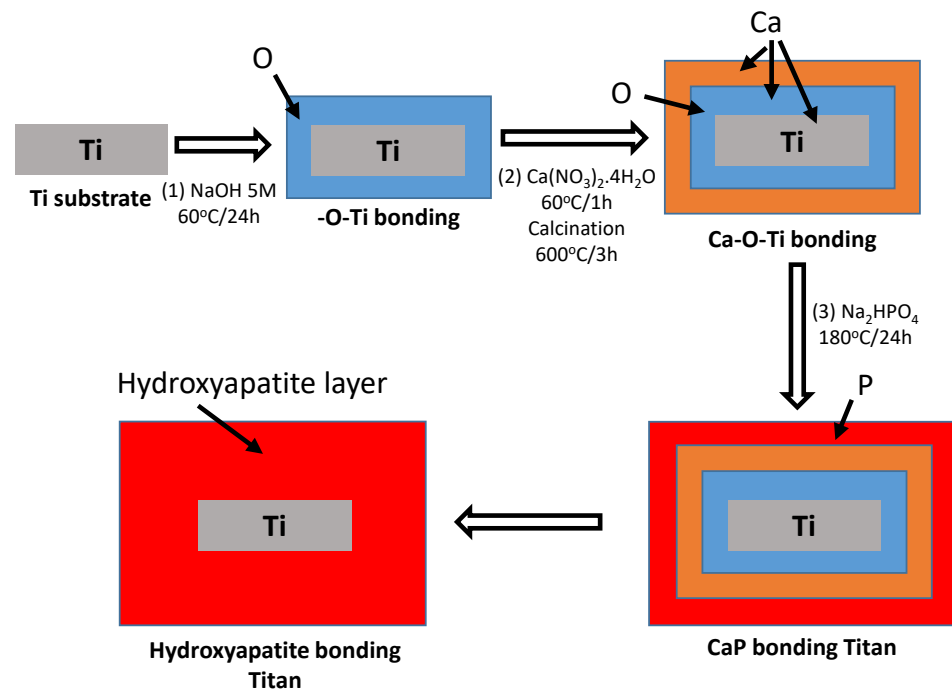


**Figure 7.** Summary layout of HA coating on the surface of Ti substrate by precipitation and hydrothermal methods.

In addition, the use of such surface modification treatment on HA-coated Ti can be used for immediate loading [37], preimplant procedures (such as sinus lifting) [38,39], bone expansion [40], particular implants [41] or bone grafting [42]. Although this research paper does not have cell study data at the present time, the literature shows that an HA coating can improve the cell viability, in particular through stem cell stimulation [43,44]. Moreover, these HA coating layers can diminish infection and inhibit biofilm information between the implant site and host tissue, as well as be useful in systemic patients [45,46], to improve oral hygiene quality in implant maintenance [47]. The HA layer coating with the  $\text{PO}_4^{3-}$  anion group can easily bond with silver ions for antibacterial exposure, especially in light of the COVID-19 pandemic, for operative indication post-lockdown [48] or to be used in association with a laser as dental materials [49].

## 5. Conclusions

In this study, we reported the fabrication of HA-coated titanium and the effect of a phosphate solution and hydrothermal treatment condition on the characteristics of hydroxyapatite-coated titanium substrate. The Ti substrate was coated with a calcium layer, then immersed in  $\text{Na}_2\text{HPO}_4$  2 M solution at 180 °C for 48 h to form HA-coated titanium. The HA-coated titanium sample seems to be a promising implant for medical applications such as immediate loading, preimplant procedures (such as sinus lifting), bone expansion, or bone grafting. The HA-coated Ti show the potential to improve the survival and success of implants placed in regenerated bone. In a future study, *in vitro* and *in vivo* analyses will be conducted to validate the potential medical applications of HA-coated titanium.



**Author Contributions:** Conceptualization, P.T.K.; investigation, P.T.K., L.H.T.A., T.N.Q.; resources, L.H.T.A., T.N.Q., P.T.K.; writing—review and editing, P.T.K. All authors have read and agreed to the published version of the manuscript.

**Funding:** This research received no external funding.

**Institutional Review Board Statement:** Not applicable.

**Informed Consent Statement:** Not applicable.

**Data Availability Statement:** Not applicable.

**Acknowledgments:** We would like to thank Ho Chi Minh City University of Technology (HCMUT), VNU-HCM for the support of time and facilities for this study.

**Conflicts of Interest:** The authors declare no conflict of interest.

## References

1. Li, Y.H.; Yang, C.; Zhao, H.D.; Qi, S.; Li, X.; Li, Y. New developments of Ti-based alloys for biomedical applications. *Materials* **2014**, *7*, 1709–1800. [[CrossRef](#)]
2. Elias, C.N.; Lima, J.H.C.; Valiev, R.; Meyers, M.A. Biomedical applications of titanium and its alloys. *J. Miner. Met. Mater. Soc.* **2008**, *60*, 46–49. [[CrossRef](#)]
3. Albrektsson, T.; Branemark, P.I.; Hansson, H.A.; Lindstrom, J. Osseointegrated titanium implants: Requirements for ensuring a long-lasting, direct bone-to-implant anchorage in man. *Acta Orthop. Scand.* **1981**, *52*, 155–170. [[CrossRef](#)]
4. Sul, Y.T. The significance of the surface properties of oxidized titanium to the bone response: Special emphasis on potential biochemical bonding of oxidized titanium implant. *Biomaterials* **2003**, *24*, 3893–3907. [[CrossRef](#)]
5. Albrektsson, T.; Johansson, C. Osteoinduction, osteoconduction and osseointegration. *Eur. Spine J.* **2001**, *10*, 96–101. [[CrossRef](#)]
6. Oyane, A.; Kim, H.M.; Furuya, T.; Kokubo, T.; Miyazaki, T.; Nakamura, T. Preparation and assessment of revised simulated body fluids. *J. Biomed. Mater. Res. A* **2003**, *65*, 188–195. [[CrossRef](#)] [[PubMed](#)]
7. Wang, L.; Hu, X.; Ma, X.; Ma, Z.; Zhang, Y.; Lu, Y.; Li, X.; Lei, W.; Feng, Y. Promotion of osteointegration under diabetic conditions by tantalum coating-based surface modification on 3-dimensional printed porous titanium implants. *Colloids Surf. B Biointerfaces* **2016**, *148*, 440–452. [[CrossRef](#)]
8. Kasemo, B.; Gold, J. Implant surfaces and interface processes. *Adv. Dent. Res.* **1999**, *13*, 8–20. [[CrossRef](#)]
9. Ordikhani, F.; Tamjid, E.; Simchi, A. Characterization and antibacterial performance of electrodeposited chitosan-vancomycin composite coatings for prevention of implant-associated infections. *Mater. Sci. Eng. C* **2014**, *41*, 240–248. [[CrossRef](#)]
10. Ferraris, S.; Spriano, S. Antibacterial titanium surfaces for medical implants. *Mater. Sci. Eng. C* **2016**, *61*, 965–978. [[CrossRef](#)]
11. Saidin, S.; Jumat, M.A.; Amin, N.A.A.M.; Hammadi, A.S.S.A. Organic and inorganic antibacterial approaches in combating bacterial infection for biomedical application. *Mater. Sci. Eng. C* **2021**, *118*, 111382. [[CrossRef](#)]
12. Croes, M.; Bakhshandeh, S.; Hengel, V.; Lietaert, K.; Kessel, K.P.M.; Pourn, B.; Wal, B.C.H.; Vogely, H.C.; Hecke, W.V.; Fluit, A.C.; et al. Antibacterial and immunogenic behavior of silver coatings on additively manufactured porous titanium. *Acta Biomater.* **2018**, *81*, 315–327. [[CrossRef](#)]
13. Liu, X.; Chu, P.K.; Ding, C. Surface modification of titanium, titanium alloys, and related materials for biomedical applications. *Mater. Sci. Eng. R Rep.* **2004**, *47*, 49–121. [[CrossRef](#)]
14. Lee, T.C.; Abdullah, H.Z.; Koshy, P.; Idris, M.I. Ultraviolet-assisted biomimetic coating of bone-like apatite on anodised titanium for biomedical applications. *Thin Solid Film.* **2018**, *660*, 191–198. [[CrossRef](#)]
15. Patel, N.R.; Gohil, P.P. A review on biomaterials: Scope, applications & human anatomy significance. *Int. J. Emerg. Technol. Adv. Eng.* **2012**, *2*, 91–101.
16. Piotrowski, B.; Baptista, A.A.; Patoor, E.; Bravetti, P.; Eberhardt, A.; Laheurte, P. Interaction of bone–dental implant with new ultra low modulus alloy using a numerical approach. *Mater. Sci. Eng. C* **2014**, *38*, 151–160. [[CrossRef](#)]
17. Akanksha, M.; Rajvi, N.; Sunil, K.M.; Ramesh, C. Stress distribution around different abutments on titanium and CFR-PEEK implant with different prosthetic crowns under parafunctional loading: A 3D FEA study. *J. Oral Biol. Craniofacial Res.* **2021**, *11*, 313–320. [[CrossRef](#)]
18. Lebre, F.; Sridharan, R.; Sawkins, M.J.; Kelly, D.J.; Brien, F.J.O.; Lavelle, E.C. The shape and size of hydroxyapatite particles dictate inflammatory responses following implantation. *Sci. Rep.* **2017**, *7*, 2922. [[CrossRef](#)] [[PubMed](#)]
19. Goodman, S.B.; Yao, Z.; Keeney, M.; Yang, F. The future of biologic coatings for orthopaedic implants. *Biomaterials* **2013**, *34*, 3174–3183. [[CrossRef](#)] [[PubMed](#)]
20. Vahabzadeh, S.; Roy, M.; Bandyopadhyay, A.; Bose, S. Phase stability and biological property evaluation of plasma sprayed hydroxyapatite coatings for orthopedic and dental applications. *Acta Biomater.* **2015**, *17*, 47–55. [[CrossRef](#)]
21. Mano, T.; Ueyama, Y.; Ishikawa, K.; Matsumura, T.; Suzuki, K. Initial tissue response to a titanium implant coated with apatite at room temperature using a blast coating method. *Biomaterials* **2002**, *23*, 1931–1936. [[CrossRef](#)]
22. Ong, J.; Appleford, M.; Oh, S.; Yang, Y.; Chen, W.H.; Bumgardner, J.D.; Haggard, W.O. The characterization and development of bioactive hydroxyapatite coatings. *J. Miner. Met. Mater. Soc.* **2006**, *58*, 67–69. [[CrossRef](#)]

23. Munting, E. The contributions and limitations of hydroxyapatite coatings to implant fixation: A histomorphometric study of load bearing implants in dogs. *Int. Orthop.* **1996**, *20*, 1–6. [[CrossRef](#)]
24. Bloebaum, R.D.; Beeks, D.; Dorr, L.D.; Savory, C.G.; Pont, J.A.D.; Hofmann, A.A. Complications with hydroxyapatite particulate separation in total hip arthroplasty. *Clin. Orthop. Relat. Res.* **1994**, *298*, 19–26.
25. Kien, P.T.; Dai Phu, H.; Linh, N.V.V.; Quyen, T.N.; Hoa, N.T. Recent Trends in Hydroxyapatite (HA) Synthesis and the Synthesis Report of Nanostructure HA by Hydrothermal Reaction. *Adv. Exp. Med. Biol.* **2018**, *1077*, 343–354. [[CrossRef](#)]
26. Oratai, J.; Nuchara, W.; Nicha, S.; Pham, T.K.; Benjaporn, I. Effects of Solid Loadings and Silica Addition on Microstructure and Compressive Strength of Hydroxyapatite Specimens Fabricated by Freeze Casting Technique. *Ceram. Int.* **2018**, *44*, 156–160. [[CrossRef](#)]
27. Pham, T.K.; Tsuru, K.; Kunio, I. Setting reaction of  $\alpha$ -TCP spheres and an acidic calcium phosphate solution for the fabrication of fully interconnected macroporous calcium phosphate. *Ceram. Int.* **2015**, *41*, 13525–13531. [[CrossRef](#)]
28. Kien, P.T.; Minh, D.Q.; Thanh, P.T.L. Iron-free hydroxyapatite powder from synthetic  $\text{Ca}(\text{OH})$  and commercialized  $\text{Ca}(\text{OH})_2$ . *Adv. Mater. Res.* **2014**, *858*, 103–110. [[CrossRef](#)]
29. Kunio, I.; Kanji, T.; Trung, K.P.; Michito, M.; Shigeki, M. Fully-interconnected Pore Forming Calcium Phosphate Cement. *Key Eng. Mater.* **2012**, *493*, 832–835. [[CrossRef](#)]
30. Pham, T.K.; Michito, M.; Kanji, T.; Shigeki, M.; Kunio, I. Effect of phosphate solution on setting reaction of  $\alpha$ -TCP spheres. *J. Aust. Ceram. Soc.* **2010**, *46*, 63–67.
31. Yujiro, D.; Hiroto, I.; Masahiro, S.; Toru, D.; Nobuo, T.; Satoshi, S.; Shutaro, S.; Daiki, I.; Kanji, T.; Kunio, I.; et al. Titanium surface treatment by calcium modification with acidetching promotes osteogenic activity and stability of dental implants. *Materialia* **2020**, *12*, 1–12. [[CrossRef](#)]
32. Liu, S.; Wang, Q.; Liu, W.; Tang, Y.; Liu, J.; Zhang, H.; Liu, X.; Liu, J.; Yang, J.; Zhang, L.C.; et al. Multi-scale Hybrid Modified Coatings on Titanium Implants for Non-cytotoxicity and Antibacterial Properties. *Nanoscale* **2021**, 1–27. [[CrossRef](#)]
33. Wang, Q.; Zhou, P.; Liu, S.; Attarilar, S.; Ma, R.L.; Zhong, Y.; Wang, L. Multi-Scale Surface Treatments of Titanium Implants for Rapid Osseointegration: A Review. *Nanomaterials* **2020**, *10*, 1244. [[CrossRef](#)]
34. Ayukawa, Y.; Takeshita, F.; Inoue, T. An immunoelectron microscopic localization of noncollagenous bone proteins (osteocalcin and osteopontin) at the bone–titanium interface of rat tibiae. *J. Biomed. Mater. Res.* **1998**, *41*, 111–119. [[CrossRef](#)]
35. Ishikawa, K.; Miyamoto, Y.; Takechi, M.; Ueyama, Y.; Suzuki, K.; Nagayama, M.; Matsumura, T. Effects of neutral sodium hydrogen phosphate on setting reaction and mechanical strength of hydroxyapatite putty. *J. Biomed. Mater. Res.* **1999**, *44*, 322–329. [[CrossRef](#)]
36. Arief, C.; Michito, M.; Kanji, T.; Shigeki, M.; Kunio, I. Fabrication of bone cement that fully transforms to carbonate apatite. *Dent. Mater. J.* **2015**, *34*, 394–401. [[CrossRef](#)]
37. Capparé, P.; Vinci, R.; Di Stefano, D.A.; Traini, T.; Pantaleo, G.; Gherlone, E.F.; Gastaldi, G. Correlation between Initial BIC and the Insertion Torque/Depth Integral Recorded with an Instantaneous Torque-Measuring Implant Motor: An in vivo Study. *Clin. Implant Dent. Relat. Res.* **2015**, *17*, 613–620. [[CrossRef](#)]
38. Crespi, R.; Capparé, P.; Gherlone, E. Sinus floor elevation by osteotome: Hand mallet versus electric mallet. A prospective clinical study. *Int. J. Oral Maxillofac. Implant.* **2012**, *27*, 1144–1150.
39. Crespi, R.; Capparé, P.; Gherlone, E. Osteotome sinus floor elevation and simultaneous implant placement in grafted biomaterial sockets: 3 years of follow-up. *J. Periodontol.* **2010**, *81*, 344–349. [[CrossRef](#)]
40. Crespi, R.; Capparé, P.; Polizzi, E.; Gherlone, E.F. Tissue remodeling after bone expansion in grafted and ungrafted sockets. *Int. J. Oral Maxillofac. Implant.* **2014**, *29*, 699–704. [[CrossRef](#)]
41. Crespi, R.; Capparé, P.; Polizzi, E.; Gherlone, E. Fresh-Socket Implants of Different Collar Length: Clinical Evaluation in the Aesthetic Zone. *Clin. Implant Dent. Relat. Res.* **2015**, *17*, 871–878. [[CrossRef](#)]
42. Vinci, R.; Tetè, G.; Lucchetti, F.R.; Capparé, P.; Gherlone, E. Implant survival rate in calvarial bone grafts: A retrospective clinical study with 10 year follow-up. *Clin. Implant Dent. Relat. Res.* **2019**, *21*, 662–668. [[CrossRef](#)] [[PubMed](#)]
43. Capparé, P.; Tetè, G.; Sberna, M.T.; Panina-Bordignon, P. The Emerging Role of Stem Cells in Regenerative Dentistry. *Curr. Gene Ther.* **2020**, *20*, 259–268. [[CrossRef](#)]
44. Tete, G.; Orto, B.; Nagni, M.; Agostinacchio, M.; Polizzi, E.; Agliardi, E. Role of induced pluripotent stem cells (IPSCS) in bone tissue regeneration in dentistry: A narrative review. *J. Biol. Regul. Homeost. Agents* **2020**, *34*, 1–10. [[PubMed](#)]
45. Cazzaniga, G.; Ottobelli, M.; Ionescu, A.; Paolone, G.; Gherlone, E.; Ferracane, J.L.; Brambilla, E. In vitro biofilm formation on resin-based composites after different finishing and polishing procedures. *J. Dent.* **2017**, *67*, 43–52. [[CrossRef](#)]
46. Gherlone, E.; Capparé, P.; Tecco, S.; Polizzi, E.; Pantaleo, G.; Gastaldi, G.; Grusovin, M.G. A Prospective Longitudinal Study on Implant Prosthetic Rehabilitation in Controlled HIV-Positive Patients with 1-Year Follow-Up: The Role of CD4+ Level, Smoking Habits, and Oral Hygiene. *Clin. Implant Dent. Relat. Res.* **2016**, *18*, 955–964. [[CrossRef](#)]
47. Tecco, S.; Grusovin, M.; Sciara, S.; Bova, F.; Pantaleo, G.; Capparé, P. The association between three attitude-related indexes of oral hygiene and secondary implant failures: A retrospective longitudinal study. *Int. J. Dent. Hyg.* **2018**, *16*, 372–379. [[CrossRef](#)] [[PubMed](#)]
48. Gherlone, E.; Polizzi, E.; Tate, G.; Capparé, P. Dentistry and Covid-19 pandemic: Operative indications post-lockdown. *The new microbiologica* **2021**, *44*, 1–11.

- 
49. Polizzi, E.; Tetè, G.; Targa, C.; Salviato, B.; Ferrini, F.; Gastaldi, G. Evaluation of the Effectiveness of the Use of the Diode Laser in the Reduction of the Volume of the Edematous Gingival Tissue after Causal Therapy. *Int. J. Environ. Res. Public Health* **2020**, *17*, 6192. [[CrossRef](#)]